bioRxiv preprint first posted online May. 7, 2018; doi: http://dx.doi.org/10.1101/311035. The copyright holder for this preprint (which was not peer-reviewed) is the author/funder, who has granted bioRxiv a license to display the preprint in perpetuity. It is made available under a CC-BY-NC-ND 4.0 International license.

Optic nerve intraneural stimulation allows selective visual cortex activation

Vivien Gaillet[1], Annarita Cutrone[2], Paola Vagni[1], Fiorenzo Artoni[2,3], Sandra Alejandra Romero Pinto[1], Dario Lipucci Di Paola[2], Silvestro Micera[2,3] and Diego Ghezzi[1]

[1] Medtronic Chair in Neuroengineering, Center for Neuroprosthetics and Institute of Bioengineering, School of Engineering, École Polytechnique Fédérale de Lausanne, Switzerland

[2] The BioRobotics Institute, Scuola Superiore Sant'Anna, Italy

[3] Bertarelli Foundation Chair in Translational Neuroengineering, Center for Neuroprosthetics and Institute of Bioengineering, School of Engineering, École Polytechnique Fédérale de Lausanne, Switzerland

Vivien Gaillet and Annarita Cutrone contributed equally to this work.

Correspondence and requests for materials should be addressed to S.M. (emails: silvestro.micera@epfl.ch, silvestro.micera@santannapisa.it) or D.G. (email: diego.ghezzi@epfl.ch).

Abstract

Retinal prostheses have been developed to restore a functional form of vision in patients affected by outer retinal layer dystrophies. Other approaches, namely optic nerve, thalamic, and cortical prostheses are under investigation to expand this toolbox both as clinical devices and as tools for fundamental research. Optic nerve stimulation is attractive since it bypasses the entire retinal network and directly activates nerve fibers. At the same time, it still takes advantage of the high-level information processing occurring downstream in the visual cortex. Here we show that a new intraneural electrode array (OpticSELINE) is effective in inducing the activation of the visual cortex upon electrical stimulation of the optic nerve. We also demonstrate that intraneural optic nerve stimulation induces selective cortical activation patterns depending on the stimulating electrode, thus suggesting that the OpticSELINE possesses spatial selectivity in fiber stimulation. In conclusion, the

bioRxiv preprint first posted online May. 7, 2018; doi: http://dx.doi.org/10.1101/311035. The copyright holder for this preprint (which was not peer-reviewed) is the author/funder, who has granted bioRxiv a license to display the preprint in perpetuity. It is made available under a CC-BY-NC-ND 4.0 International license.

1 OpticSELINE can be used both as visual prosthesis for blind patients and as tool to further investigate

2 the effect of the electrical stimulation in the visual system.

bioRxiv preprint first posted online May. 7, 2018; doi: http://dx.doi.org/10.1101/311035. The copyright holder for this preprint (which was not peer-reviewed) is the author/funder, who has granted bioRxiv a license to display the preprint in perpetuity. It is made available under a CC-BY-NC-ND 4.0 International license.

1 Visual prostheses recently emerged as tool to fight blindness; a medical condition affecting more than
2 30 million people worldwide [1]. Starting from early pioneering works [2,3], over the past 50 years several
3 types of visual prostheses have been proposed and classified by their location along the visual
4 pathway [4,5], including: subretinal [6], epiretinal [7], suprachoroidal [8], optic nerve [9], thalamic [10], and
5 cortical prostheses [11]. Retinal implants quickly became the preferred strategies, since they can benefit
6 from the natural information processing along the visual pathway, despite the limit to treat only
7 diseases affecting retinal photoreceptors [12]. In various clinical trials, retinal prostheses demonstrated
8 the capability to restore a functional form of vision [13,14], and today several research groups are
9 developing novel retinal prostheses [15–17]. On the other hand, cortical prostheses are still facing several
10 technical and biological challenges; the invasiveness of surgical implantation, the risk of focal seizures
11 induced by direct cortical stimulation, and the requirement of high-level information coding pose
12 serious concerns for their clinical application [12,18]. On the contrary, optic nerve stimulation is
13 attractive since it bypasses the entire retinal network and directly activates nerve fibers. At the same
14 time, it still takes advantage of the high-level information processing occurring in the visual cortex.
15 Optic nerve stimulation has been pioneered with the implantation of a 4-contact epineural electrode in
16 the intra-cranial trait of a blind subject [19], in which electrical stimuli have been able to elicit localized
17 phosphenes. After few months of training and psychophysical testing, the patient has been able to
18 distinguish line orientations as well as shapes and symbols despite using only 4 electrodes. Another
19 patient has been implanted later with a 8-contact electrode [20], confirming the possibility of restoring
20 functional vision by using optic nerve stimulation [21–23]. However, in those trials the induced
21 phosphenes have been reported as irregulars; the use of epineural electrodes may be the cause [24], due
22 to their limited mechanical stability. Following this approach, an optic nerve prosthesis is currently
23 under investigation by the C-Sight project, which is testing the stimulation of the intra-orbital region
24 with a 4-filament electrode; acute results have been documented in rabbits [25,26] and cats [27]. This
25 project employs penetrating platinum-iridium electrodes, which are characterized by high stiffness
26 inducing a large mechanical mismatch with the nerve; in turn this may have consequences for chronic
27 implantation. On the contrary, transverse intra-fascicular multichannel electrode (TIME) arrays,
28 micro-fabricated via thin-film technology, have already demonstrated their superior capability in

bioRxiv preprint first posted online May. 7, 2018; doi: http://dx.doi.org/10.1101/311035. The copyright holder for this preprint (which was not peer-reviewed) is the author/funder, who has granted bioRxiv a license to display the preprint in perpetuity. It is made available under a CC-BY-NC-ND 4.0 International license.

1 several applications related to nerve stimulation[28,29]. Indeed, intraneural electrodes show a higher
2 selectivity in fiber stimulation[30,31] with respect to epineural electrodes. More recently, a self-opening
3 intraneural electrode (SELINE) demonstrated its improved mechanical stability[32] and
4 biocompatibility over a period of 6 months[33]. In this work, a modified version of the previously
5 described SELINE electrode array[32,33], has been successfully exploited as visual prosthesis based on
6 optic nerve stimulation.
7
8 **Results**
9 ***Electrode design and characterization***. The OpticSELINE is a polyimide-based looped structure with
10 a total length of 33 mm, a maximum width of 3 mm, and an overall thickness of 0.012 mm (**Fig. 1a**). A
11 polyimide-based extension flat cable of 35 mm allows the connection between the electrode and the
12 head-plug connector. It has twelve stimulating electrodes (six electrodes per side, area of 0.008 mm^2)
13 plus a reference and a ground electrode outside the active area. Each side has two three-dimensional
14 flaps that extend from the main body and carry two electrodes each; two more electrodes are located
15 on each side of the main body. The width of the active area is 0.43 mm and the length is 1.25 mm. Each
16 flap has a width of 0.15 mm and a length of 0.48 mm (**Fig. 1b**). Four alignment bars (width of 0.1 mm)
17 have been included to ease the insertion procedure and verify that the active area is located inside the
18 optic nerve (**Fig. 1c**). The OpticSELINE has been designed in agreement with the anatomical structure
19 of the rabbit's optic nerve, which has an average (± s.e.m.) diameter of 1.45 ± 0.04 mm
20 (**Supplementary Fig. 1**).
21 The OpticSELINE has been characterized electrochemically and mechanically. First, cyclic voltammetry
22 has been performed to determine the charge storage capacity of the electrodes (**Fig. 2a**). This test has
23 been executed before and after an accelerated ageing time equivalent to an implantation time of 6.4
24 months (6 days at 87 °C)[34]. The mean charge storage capacity is not significantly different before and
25 after ageing (**Fig. 2b**; n = 18; p = 0.1919, paired t-test). Given the small electrode area (0.008 mm^2),
26 this value of charge storage capacity is comparable to values found in literature for gold
27 microelectrodes[35]. Similarly, the impedance spectroscopy has been performed (**Fig. 2c**), and the mean

bioRxiv preprint first posted online May. 7, 2018; doi: http://dx.doi.org/10.1101/311035. The copyright holder for this preprint (which was not peer-reviewed) is the author/funder, who has granted bioRxiv a license to display the preprint in perpetuity. It is made available under a CC-BY-NC-ND 4.0 International license.

1 magnitude at 1kHz has shown non-significant statistical difference before and after ageing (**Fig. 2d**; n
2 = 30; p = 0.7613, paired t-test).
3 A mechanical characterization has been performed to verify the compatibility of the electrode array
4 with insertion forces and the stability within the nerve. During insertion experiments (**Fig. 3a**) two
5 major force peaks have been observed (**Fig. 3c,e**) corresponding to the insertion of the loop inside the
6 nerve (peak 1) and to the entry of the enlarged area of the device (peak 2). The stability of the
7 electrode within the nerve has been evaluated with an extraction experiment (**Fig. 3b**). During
8 extraction two major force peaks have been observed (**Fig. 3d,f**) corresponding to the force necessary
9 to extract the three-dimensional flaps (peak 3 and 4) followed by a flat phase relative to the slippage of
10 the loop through the nerve (5). Measured extraction forces are 25 folds larger than the forces required
11 to extract an electrode array without three-dimensional flaps, as previously measured in the rat sciatic
12 nerve [32] . This confirms that the presence of three-dimensional flaps enhances the anchorage of
13 OpticSELINE within the nerve and provides a better mechanical stability.
14 ***Visual stimulation***. Visually-evoked cortical potentials (VEPs) have been characterized in New
15 Zeeland White rabbits upon flash illumination (**Fig. 4a**). The peak amplitudes (PAs) and the peak
16 latencies (PLs) of the major peaks present in the VEP (N1 and P1) have been measured using an
17 electrocorticography (ECoG) electrode array (**Fig. 4b**). Each rabbit (N = 9) has been stimulated on both
18 eyes (ipsilateral and contralateral with respect to the ECoG array) with light flashes of increasing
19 luminance (0.1, 0.5, 1, 5, 10, and 30 cd s m^{-2}). As expected the strongest and fastest response occurs for
20 contralateral stimulation (**Fig. 4c**), since in rabbits 90 to 95 % of the fibers decussate at the level of the
21 chiasma [36] . Similar to a previous report [37] , the average (± s.e.m.) P1 PL in contralateral stimulation
22 (**Fig. 4d**) starts at 33.93 ± 2.59 ms for low luminance (0.1 cd s m^{-2}) and reaches a plateau latency of
23 23.28 ± 1.86 ms for higher luminance (5 cd s m^{-2}). Also, N1 PL in contralateral stimulation is
24 comparable to previously reported data (29.41 ± 2.40 ms, 25.17 ± 2.17 ms, 24.46 ± 2.01 ms, 20.65 ±
25 2.79 ms, 19.80 ± 1.35 ms, and 20.00 ± 1.38 ms respectively for 0.1, 0.5, 1, 5, 10, and 30 cd s m^{-2}).
26 ***Electrical stimulation***. The OpticSELINE has been implanted transversally in the optic nerve from the
27 lateral to the medial side. Because of fiber decussation [36] , electrically-evoked cortical potentials (EEPs)
28 have been measured with an ECoG array only in the contralateral visual cortex (**Fig. 5a,b**). Cathodic

bioRxiv preprint first posted online May. 7, 2018; doi: http://dx.doi.org/10.1101/311035. The copyright holder for this preprint (which was not peer-reviewed) is the author/funder, who has granted bioRxiv a license to display the preprint in perpetuity. It is made available under a CC-BY-NC-ND 4.0 International license.

1 first asymmetrically balanced (1:5) electrical stimuli have been used. The ratio 1:5 has been previously
2 demonstrated to be a good compromise between total pulse duration and stimulation efficiency [26] . In
3 the same study, it has been also shown that placing the balancing anodic phase before the cathodic
4 stimulation phase with a 1:5 ration has no influence. Moreover, we did not introduce any inter-phase
5 gap since it has been demonstrated to have a significant effect only with symmetrically balanced
6 stimuli [26] . To avoid fatigue in the nerve due to repetitive stimulations, only 6 electrodes of the
7 OpticSELINE (1 to 6 in the top shank, from left to right) have been used in the first part of the study. In
8 this condition, nerve fatigue due to repetitive stimulation has not been observed (**Supplementary Fig.**
9 **2**).
10 Under electrical stimulation of the optic nerve we found that both N1 and P1 peak amplitudes increase
11 with the current amplitude of the stimulus (**Fig. 5c,e**). Then, we have measured the minimum current
12 required to induce the N1 peak in the cortical response (average of the 32 electrodes of the ECoG). N1
13 current threshold decreases with the increase of the pulse duration; on the contrary, the pulse
14 duration seems to have a minimal effect on the amount of charges required to activate N1 (**Fig. 5d**), as
15 previously observed [38] . Therefore, the phase duration has been fixed to 150 μs. Under this condition,
16 the mean (± s.e.m.) N1 threshold results in 204.17 μA (**Fig. 5f**). Interestingly, the electrodes on the
17 main body (numbers 3 and 4) have a mean (± s.e.m.) threshold higher (**Fig. 5g**) than the electrodes on
18 the flaps (numbers 1, 2, 5, and 6). This could be explained since in the pre-chiasmatic trait of the optic
19 nerve the fibers with large diameter are localized more in the periphery of the nerve than in the center
20 (**Supplementary Fig. 3**).
21 Retinal ganglion cells can generate action potentials up to few hundreds of Hz; for such reason, the
22 artificial reproduction of this code requires high frequency electrical pulsing. We verified the
23 possibility to use high frequency pulse trains (1, 2, 3, or 4 pulses at 1 kHz of repetition rate) for optic
24 nerve stimulation (**Fig. 6a**). By increasing the number of pulses within the train (from 1 to 4) at
25 constant current amplitude, the mean (± s.e.m.) N1 threshold is progressively reduced down to 46.15
26 ± 11.79 % (for 4 pulses) of the threshold obtained with a single pulse (**Fig. 6b**). Similarly, the cortical
27 activation (e.g. P1 PA) can be modulated by increasing the number of pulses instead of changing the
28 current intensity (**Fig. 6c**).

bioRxiv preprint first posted online May. 7, 2018; doi: http://dx.doi.org/10.1101/311035. The copyright holder for this preprint (which was not peer-reviewed) is the author/funder, who has granted bioRxiv a license to display the preprint in perpetuity. It is made available under a CC-BY-NC-ND 4.0 International license.

1 **Stimulation selectivity**. Last, we investigated the spatial selectivity of intraneural stimulation of the
2 optic nerve with single pulses. A blind source separation approach has been used to quantitatively
3 extract differences between the EEPs resulting from the stimulation through different electrodes of
4 the OpticSELINE. Independent component analysis (ICA)[39] has been chosen since it is steadily gaining
5 popularity among blind source separation techniques to disentangle information linearly mixed into
6 multiple recorded data channels so as to prepare multivariate data sets for more general data mining
7 [40–42].

8 We hypothesized that each EEP is composed of 'shared' components and 'meaningful' components: the
9 former ones are characterized by similar time courses regardless of the stimulating electrode
10 activated in the OpticSELINE, while the latter ones have time courses that are specific to one specific
11 stimulating electrode (or to a small subset at maximum). ICA has been performed on the 32 ECoG
12 recordings in order to highlight the presence of meaningful components that may have dispersed in
13 the common cortical signal. ICA linearly projects the 32 original time courses into 32 new maximally-
14 independent time courses, here called independent components (ICs), as weighted sums of the
15 original time courses. The region of the visual cortex in which each IC is present has been determined
16 by plotting the activation map (see Methods) of each IC on the 32 electrodes of the recording array
17 (**Fig. 7a**). In addition, ICs have been classified in different categories, based on their time course
18 (**Supplementary Fig. 4**), namely: artifact (i.e., containing the stimulation artifact), noise (i.e.,
19 containing a high frequency signal), flat (i.e., not containing any peaks in their waveform), common
20 (i.e., having a similar time courses for each of the stimulating channels), and meaningful (i.e., having
21 different time courses depending on the stimulating channel). In a representative example (N = 1
22 rabbit, current amplitude of 750 μA), amongst the 32 ICs, 26 have been labelled as meaningful, 2 as
23 common, 1 as flat, 1 as noise, and 2 as artifact (**Fig. 7b**, **Supplementary Fig. 5**). In this representative
24 example 9 stimulating channels out of 12 resulted in a meaningful cortical activation, while 3 of them
25 induced flat responses only. By back-projecting only the meaningful ICs onto the original channel
26 space, the original data can be also filtered to highlight only the meaningful component
27 (**Supplementary Fig. 6**). By increasing the current amplitude of the pulse, the number of ICs classified
28 as meaningful increases, it reaches his maximum value (26) at 500 μA until 1000 μA, and then

bioRxiv preprint first posted online May. 7, 2018; doi: http://dx.doi.org/10.1101/311035. The copyright holder for this preprint (which was not peer-reviewed) is the author/funder, who has granted bioRxiv a license to display the preprint in perpetuity. It is made available under a CC-BY-NC-ND 4.0 International license.

1 decreases (**Supplementary Fig. 7b**). This is probably due to the beginning of the saturation of the
2 cortical response; therefore, more ICs are classified as common instead of meaningful.
3 The activation maps of the 26 meaningful ICs show that they are present in distinct regions of the
4 visual cortex, which suggests that the components of the original signal are spatially segregated in the
5 visual cortex (**Fig. 7c**). In addition, each meaningful ICs exhibits a different degree of activation
6 depending on the stimulating electrode used. To quantify this, for each meaningful IC, the peak-to-
7 peak amplitude of the early portion of the time courses (from 5 to 25 ms after the pulse) induced by
8 each stimulating electrode was computed and normalized amongst all the stimulating electrodes. All of
9 the 9 stimulating electrodes have at least one meaningful IC whose activation is maximized when
10 stimulating through this particular electrode. Furthermore, by interpolating the contribution of every
11 stimulating electrode to each IC, we found their distribution map within the optic nerve (**Fig. 8a** and
12 **Supplementary Fig. 8**). The area corresponding to 90 % of the activation level (red lines) is confined
13 to a small area around this electrode, or in few cases it spreads over 1 or 2 neighboring electrodes (**Fig.
14 8b**). The spatial segregation of the ICs at the level of the visual cortex (**Fig. 7**) and the high localization
15 of ICs in correspondence of the OpticSELINE electrodes (**Fig. 8**) are considered indirect signatures that
16 the different stimulating electrodes recruit different population of optic nerve fibers, thus confirming
17 that the OpticSELINE allows selective visual cortex activation.
18

19 **Discussion**

20 Currently, the research on visual prostheses is largely focused on the development of novel retinal
21 prosthesis [15–17,43–47] , either subretinal, epiretinal, or suprachoroidal. Nevertheless, beside the early
22 pioneering works, some research groups are now attempting the stimulation of downstream regions
23 of the visual pathway [12] . Among those, optic nerve prostheses aim at stimulating the axonal fibers
24 from retinal ganglion cells during their pathway towards the optic chiasma. Following two initial
25 studies on two blind patients affected by Retinitis pigmentosa [19,20] , optic nerve stimulation is now
26 under validation in a clinical trial by another group which is targeting the optic disk in the retina [48] .
27 In the first clinical trial, the two patients have been implanted with epineural cuff electrodes, which
28 are less invasive than intraneural arrays. However, epineural electrodes mostly target external fibers,

bioRxiv preprint first posted online May. 7, 2018; doi: http://dx.doi.org/10.1101/311035. The copyright holder for this preprint (which was not peer-reviewed) is the author/funder, who has granted bioRxiv a license to display the preprint in perpetuity. It is made available under a CC-BY-NC-ND 4.0 International license.

1 while intraneural electrodes can stimulate also the central area of the nerve and provide higher
2 selectivity [31] . In addition, intraneural electrodes are mechanically more stable than epineural [32] ,
3 therefore allowing a more reproducible and stable stimulation. For this reason, we selected an
4 intraneural approach, confirming mechanical stability, due also to the lateral flaps, and selectivity in
5 fiber recruitment as demonstrated by the blind source separation analysis.

6 In our experimental design, we choose to target the intra-cranial trait of the optic nerve. Epineural
7 electrodes have been previously implanted in both the intra-orbital [20] and intra-cranial trait of the
8 nerve [19] . The comparison of the two clinical studies showed that intra-orbital stimulation induces
9 smaller EEPs with respect to intra-cranial stimulation, while latencies are not significantly different; in
10 other words, the perceptual threshold is higher for intra-orbital stimulation [9] . In addition, the intra-
11 orbital trait of the optic nerve must accommodate the eye movements; therefore, an intraneural
12 electrode may be subjected to high cyclic strain which may later lead to failure. This is minimized in
13 the intra-cranial trait. A second drawback of the intra-orbital placement of an intraneural electrode is
14 due to the presence of the central retinal vein and artery entering the nerve approximately 1 cm far
15 from the eye bulb; therefore, an intraneural placement may risk to damage them. Therefore, intra-
16 cranial stimulation by intraneural electrodes seems more appropriate than intra-orbital stimulation.

17 Compared to retinal prostheses, and in particular epiretinal implants, optic nerve stimulation differs
18 since it activates only axonal fibers. During epiretinal stimulation, electric pulses may induce a direct
19 activation of retinal ganglion cell fibers or an indirect activation via the internal retinal circuit. It is
20 known that brief (hundreds of μs) cathodic epiretinal stimulation preferentially excites the axons of
21 retinal ganglion cells, while pulses longer than 1 ms excite both retinal ganglion cells and bipolar cells
22 [16,49,50] . A recent study has demonstrated that the increase of the stimulation to 25 ms per phase
23 significantly reduces the unwanted activation of axon of passage. In turns, this enhances the indirect
24 activation or retinal ganglion cells via the internal retinal circuits, which provides a more focal
25 activation avoiding streak responses [51] . The disadvantage of long stimulations (25 ms per phase) is
26 the reduction of the frame rate available. Currently the Argus II operates in the range of 3 to 60 Hz [52]
27 ; however, the increase of the pulse duration to 25 ms may limit the maximum frame rate to about 10
28 Hz. An attractive strategy for visual prostheses is neuromorphic encoding [53–55] , where the conversion

bioRxiv preprint first posted online May. 7, 2018; doi: http://dx.doi.org/10.1101/311035. The copyright holder for this preprint (which was not peer-reviewed) is the author/funder, who has granted bioRxiv a license to display the preprint in perpetuity. It is made available under a CC-BY-NC-ND 4.0 International license.

1 between an image and the pattern of electrical stimulation delivered to the tissue is based on an in-
2 silico morphing of the retinal process. In this case the stimulation pattern delivered to the neurons
3 (e.g. retinal ganglion cells) can be a representation of the natural code. Retinal ganglion cells can fire
4 action potentials up to few hundreds of Hz, therefore the reproduction of this natural code may
5 require a high temporal precision. It is now evident that an epiretinal strategy may not combine the
6 use of long pulses (e.g. 25 ms per phase) with a neuromorphic approach. On the contrary we have
7 demonstrated that optic nerve stimulation can be implemented at high frequency (i.e., 1 kHz) thus
8 allowing the reproduction of the natural code of retinal ganglion cells with high temporal fidelity.
9 Optic nerve stimulation appears as good strategy for neuromorphic prostheses or for the testing of
10 neuromorphic algorithms in animal models.

11 An important aspect to enable the OpticSELINE as visual prosthesis is the capability to induce selective
12 optic nerve stimulation and generate spatially organized phosphenes. The first clinical trial with
13 epineural electrodes already demonstrated that optic nerve stimulation may induce spatially
14 organized phosphenes [22] . The C-Sight project demonstrated in rabbits that the position of the cortical
15 channel with the highest amplitude can be spatially modulated by applying current-steering methods
16 to the intraneural stimulation of the intra-orbital trait of the optic nerve [25] . We have found that with
17 an intraneural multi-electrode array is possible to associate 'meaningful' cortical activation patterns
18 with specific electrodes of the array, confirming that the OpticSELINE induces activation of the visual
19 cortex in a reproducible and spatially organized manner. This is possible because of the selective
20 activation of nerve fibers, which could open the possibility to elicit behaviorally relevant visual
21 activation patterns by optimizing the stimulation protocol. This represents a fundamental
22 breakthrough towards the implantation of the optic nerve stimulation to restore functional vision.

23

24 **References**

25 1. Bourne, R. *et al.* Causes of vision loss worldwide, 1990-2010: a systematic analysis. *The*
26 *Lancet. Global health* **1,** e339–49 (2013).
27 2. Brindley & Lewin. The sensations produced by electrical stimulation of the visual cortex.
28 *The Journal of physiology* **196,** 479–93 (1968).
29 3. Dobelle, Mladejovsky & Girvin. Artificial Vision for the Blind: Electrical Stimulation of
30 Visual Cortex Offers Hope for a Functional Prosthesis. *Science* **183,** 440–444 (1974).

bioRxiv preprint first posted online May. 7, 2018; doi: http://dx.doi.org/10.1101/311035. The copyright holder for this preprint (which was not peer-reviewed) is the author/funder, who has granted bioRxiv a license to display the preprint in perpetuity. It is made available under a CC-BY-NC-ND 4.0 International license.

1 4. Zrenner, E. Fighting Blindness with Microelectronics. *Science Translational Medicine* **5,**
2 210ps16 (2013).
3 5. Ghezzi, D. Retinal prostheses: progress toward the next generation implants. *Frontiers in*
4 *neuroscience* **9,** 290 (2015).
5 6. Stingl, K. *et al.* Artificial vision with wirelessly powered subretinal electronic implant
6 alpha-IMS. *Proceedings. Biological sciences / The Royal Society* **280,** 20130077 (2013).
7 7. Da Cruz, L. *et al.* Five-Year Safety and Performance Results from the Argus II Retinal
8 Prosthesis System Clinical Trial. *Ophthalmology* **123,** 2248–2254 (2016).
9 8. Ayton, L. *et al.* First-in-human trial of a novel suprachoroidal retinal prosthesis. *PloS one* **9,**
10 e115239 (2014).
11 9. Brelén, M., Vince, V., Gérard, B., Veraart, C. & Delbeke, J. Measurement of Evoked
12 Potentials after Electrical Stimulation of the Human Optic Nerve. *Investigative Ophthalmology &*
13 *Visual Science* **51,** 5351–5355 (2010).
14 10. Panetsos, F., Sanchez-Jimenez, A., Cerio, E., Diaz-Guemes, I. & Sanchez, F. Consistent
15 phosphenes generated by electrical microstimulation of the visual thalamus. An experimental
16 approach for thalamic visual neuroprostheses. *Frontiers in neuroscience* **5,** 84 (2011).
17 11. Normann, R. *et al.* Toward the development of a cortically based visual neuroprosthesis.
18 *Journal of neural engineering* **6,** 035001 (2009).
19 12. Merabet, L., Rizzo, J., Amedi, A., Somers, D. & Pascual-Leone, A. What blindness can tell
20 us about seeing again: merging neuroplasticity and neuroprostheses. *Nature Reviews Neuroscience*
21 **6,** 71–77 (2005).
22 13. Luo, Y. H. & da Cruz, L. The Argus(®) II Retinal Prosthesis System. *Prog Retin Eye Res*
23 (2015). doi:10.1016/j.preteyeres.2015.09.003
24 14. Stingl, K. *et al.* Subretinal Visual Implant Alpha IMS – Clinical trial interim report. *Vision*
25 *Res* **111,** 149–160 (2015).
26 15. Lorach, H. *et al.* Photovoltaic restoration of sight with high visual acuity. *Nature Medicine*
27 **21,** 476–482 (2015).
28 16. Ferlauto, L. *et al.* Design and validation of a foldable and photovoltaic wide-field epiretinal
29 prosthesis. *Nature Communications* **9,** 992 (2018).
30 17. Maya-Vetencourt, J. F. F. *et al.* A fully organic retinal prosthesis restores vision in a rat
31 model of degenerative blindness. *Nat Mater* (2017). doi:10.1038/nmat4874
32 18. Fernández *et al.* Development of a cortical visual neuroprosthesis for the blind: the
33 relevance of neuroplasticity. *Journal of Neural Engineering* **2,** R1–12 (2005).
34 19. Veraart, C. *et al.* Visual sensations produced by optic nerve stimulation using an implanted
35 self-sizing spiral cuff electrode. *Brain Research* **813,** 181–186 (1998).
36 20. Brelén, M. *et al.* Intraorbital implantation of a stimulating electrode for an optic nerve visual
37 prosthesis. Case report. *J Neurosurg* **104,** 593–7 (2006).
38 21. Duret, F. *et al.* Object localization, discrimination, and grasping with the optic nerve visual
39 prosthesis. *Restor Neurol Neuros* **24,** 31–40 (2006).
40 22. Veraart, C., Wanet-Defalque, M., Gérard, B., Vanlierde, A. & Delbeke, J. Pattern
41 Recognition with the Optic Nerve Visual Prosthesis. **27,** 9961004 (2003).
42 23. Brelén, Duret, Gérard, Delbeke & Veraart. Creating a meaningful visual perception in blind
43 volunteers by optic nerve stimulation. *Journal of neural engineering* **2,** S22–8 (2005).
44 24. The Lasker/IRRF Initiative for Innovation in Vision Science. Restoring Vision to the Blind:
45 The New Age of Implanted Visual Prostheses. *Transl Vis Sci Technology* **3,** 3–3 (2014).
46 25. Yan, Y. *et al.* Electrically Evoked Responses in the Rabbit Cortex Induced by Current
47 Steering With Penetrating Optic Nerve Electrodes. **57,** 6327–6338 (2016).
48 26. Sun, J., Chen, Y., Chai, X., Ren, Q. & Li, L. Penetrating electrode stimulation of the rabbit
49 optic nerve: parameters and effects on evoked cortical potentials. **251,** 2545–54 (2013).
50 27. Lu, Y. *et al.* Electrical stimulation with a penetrating optic nerve electrode array elicits
51 visuotopic cortical responses in cats. **10,** 036022 (2013).

bioRxiv preprint first posted online May. 7, 2018; doi: http://dx.doi.org/10.1101/311035. The copyright holder for this preprint (which was not peer-reviewed) is the author/funder, who has granted bioRxiv a license to display the preprint in perpetuity. It is made available under a CC-BY-NC-ND 4.0 International license.

1 28. Raspopovic, S & Capogrosso, M. Restoring natural sensory feedback in real-time
2 bidirectional hand prostheses. *Science translational …* (2014). doi:10.1126/scitranslmed.3006820
3 29. Oddo, C. *et al.* Intraneural stimulation elicits discrimination of textural features by artificial
4 fingertip in intact and amputee humans. *eLife* **5,** e09148 (2016).
5 30. Raspopovic, S., Capogrosso, M., Badia, J., Navarro, X. & Micera, S. Experimental
6 validation of a hybrid computational model for selective stimulation using transverse intrafascicular
7 multichannel electrodes. *IEEE transactions on neural systems and rehabilitation engineering□: a*
8 *publication of the IEEE Engineering in Medicine and Biology Society* **20,** 395–404 (2012).
9 31. Badia, J. *et al.* Comparative analysis of transverse intrafascicular multichannel, longitudinal
10 intrafascicular and multipolar cuff electrodes for the selective stimulation of nerve fascicles.
11 *Journal of Neural Engineering* **8,** 036023 (2011).
12 32. Cutrone *et al.* A three-dimensional self-opening intraneural peripheral interface (SELINE).
13 *Journal of Neural Engineering* **12,** 016016 (2015).
14 33. Wurth *et al.* Long-term usability and bio-integration of polyimide-based intra-neural
15 stimulating electrodes. *Biomaterials* **122,** 114–129 (2017).
16 34. Hukins, D. W. L., Mahomed & Kukureka, S. N. Accelerated aging for testing polymeric
17 biomaterials and medical devices. *Medical Engineering & Physics* **30,** 1270–1274 (2008).
18 35. Howlader, M., Doyle, Mohtashami & Kish. Charge transfer and stability of implantable
19 electrodes on flexible substrate. *Sensors and Actuators B: Chemical* **178,** 132–139 (2013).
20 36. Giolli, R. A. & Guthrie, M. D. The primary optic projections in the rabbit. An experimental
21 degeneration study. *J. Comp. Neurol.* **136,** 99–126 (1969).
22 37. Sun, J. *et al.* Spatiotemporal properties of multipeaked electrically evoked potentials elicited
23 by penetrative optic nerve stimulation in rabbits. **52,** 146–54 (2011).
24 38. Li, L. *et al.* Intraorbital optic nerve stimulation with penetrating electrodes: in vivo
25 electrophysiology study in rabbits. *Graefe's Archive for Clinical and Experimental Ophthalmology*
26 **247,** 349–361 (2009).
27 39. Bell & Sejnowski. An information-maximization approach to blind separation and blind
28 deconvolution. *Neural computation* **7,** 1129–59 (1995).
29 40. Delorme, A., Palmer, J., Onton, J., Oostenveld, R. & Makeig, S. Independent EEG sources
30 are dipolar. *PloS one* **7,** e30135 (2012).
31 41. Menicucci, D. *et al.* Brain responses to emotional stimuli during breath holding and
32 hypoxia: an approach based on the independent component analysis. *Brain topography* **27,** 771–85
33 (2014).
34 42. Artoni, F. *et al.* Unidirectional brain to muscle connectivity reveals motor cortex control of
35 leg muscles during stereotyped walking. *NeuroImage* **159,** 403–416 (2017).
36 43. Ghezzi, D. *et al.* A polymer optoelectronic interface restores light sensitivity in blind rat
37 retinas. *Nat Photonics* **7,** 400–406 (2013).
38 44. Antognazza, M. R. *et al.* Characterization of a Polymer-Based, Fully Organic Prosthesis for
39 Implantation into the Subretinal Space of the Rat. *Adv Healthc Mater* **5,** 2271–82 (2016).
40 45. Mathieson, K. *et al.* Photovoltaic retinal prosthesis with high pixel density. *Nature*
41 *Photonics* **6,** 391–397 (2012).
42 46. Mandel, Y. *et al.* Cortical responses elicited by photovoltaic subretinal prostheses exhibit
43 similarities to visually evoked potentials. *Nature communications* **4,** 1980 (2013).
44 47. Tang, J. *et al.* Nanowire arrays restore vision in blind mice. *Nature Communications* **9,** 786
45 (2018).
46 48. Sakaguchi, H. *et al.* Artificial vision by direct optic nerve electrode (AV-DONE)
47 implantation in a blind patient with retinitis pigmentosa. *J Artif Organs* **12,** 206–209 (2009).
48 49. Jensen, R. J. & Rizzo, J. F. Thresholds for activation of rabbit retinal ganglion cells with a
49 subretinal electrode. *Exp. Eye Res.* **83,** 367–73 (2006).
50 50. Behrend, M., Ahuja, A., Humayun, M., Chow, R. & Weiland, J. Resolution of the epiretinal
51 prosthesis is not limited by electrode size. *IEEE transactions on neural systems and rehabilitation*

bioRxiv preprint first posted online May. 7, 2018; doi: http://dx.doi.org/10.1101/311035. The copyright holder for this preprint (which was not peer-reviewed) is the author/funder, who has granted bioRxiv a license to display the preprint in perpetuity. It is made available under a CC-BY-NC-ND 4.0 International license.

1 *engineering□: a publication of the IEEE Engineering in Medicine and Biology Society* **19,** 436–42
2 (2011).
3 51. Weitz, A. C. *et al.* Improving the spatial resolution of epiretinal implants by increasing
4 stimulus pulse duration. *Sci Transl Med* **7,** 318ra203 (2015).
5 52. Dorn, J. *et al.* The Detection of Motion by Blind Subjects With the Epiretinal 60-Electrode
6 (Argus II) Retinal Prosthesis. *JAMA Ophthalmology* **131,** 183–189 (2013).
7 53. Nirenberg, S. & Pandarinath, C. Retinal prosthetic strategy with the capacity to restore
8 normal vision. *Proceedings of the National Academy of Sciences of the United States of America*
9 **109,** 15012–7 (2012).
10 54. Piedade, M., Gerald, J., Sousa, L., Tavares, G. & Tomás, P. Visual Neuroprosthesis: A Non
11 Invasive System for Stimulating the Cortex. *Ieee Transactions Circuits Syst Regul Pap* **52,** 2648–
12 2662 (2005).
13 55. Zaghloul, K. & Boahen, K. Optic Nerve Signals in a Neuromorphic Chip II: Testing and
14 Results. *Ieee T Bio-med Eng* **51,** 667–675 (2004).
15 56. Palmer, J., Kreutz-Delgado, K., Rao, B. & Makeig, S. *Independent Component Analysis and*
16 *Signal Separation*. *Springer* **4666,** 97–104 (2007).
17 57. Artoni, F., Menicucci, D., Delorme, A., Makeig, S. & Micera, S. RELICA: a method for
18 estimating the reliability of independent components. *NeuroImage* **103,** 391–400 (2014).
19 58. Artoni, F., Delorme, A. & Makeig, S. Applying dimension reduction to EEG data by
20 principal component analysis reduces the quality of its subsequent independent component
21 decomposition. *NeuroImage* (2018). doi:10.1016/j.neuroimage.2018.03.016
22

23 **Acknowledgement**

24 This work has been supported by École Polytechnique Fédérale de Lausanne, Medtronic, Bertarelli
25 Foundation, and Wyss Center for Bio and Neuroengineering. Dr. Artoni is supported by the European
26 Union's Horizon 2020 research and innovation programme under Marie Skłodowska Curie grant
27 agreement No. 750947 (BIREHAB).

28

29 **Author contributions**

30 V.G. designed the stimulation protocol, performed data analysis and blind source separation. A.C.
31 designed and fabricated the OpticSELINE and performed mechanical and electrochemical
32 characterizations. P.V. performed in-vivo and histological experiments. F.A. performed data analysis
33 and conceived the blind source separation approach. S.A.R.P. participated in the design of the
34 stimulation protocol and in data analysis. D.L.D.P. participated in the design and microfabrication of
35 the OpticSELINE and performed mechanical characterizations. S.M. designed the study and supervised
36 the activities related to electrode development and the blind source separation approach. D.G.
37 designed the study, led the project, and wrote the manuscript. All the authors read, edited, and
38 accepted the manuscript.

39

bioRxiv preprint first posted online May. 7, 2018; doi: http://dx.doi.org/10.1101/311035. The copyright holder for this preprint (which was not peer-reviewed) is the author/funder, who has granted bioRxiv a license to display the preprint in perpetuity.
It is made available under a CC-BY-NC-ND 4.0 International license.

1 **Competing Financial Interests statement**

2 The authors declare no competing financial interests.

bioRxiv preprint first posted online May. 7, 2018; doi: http://dx.doi.org/10.1101/311035. The copyright holder for this preprint (which was not peer-reviewed) is the author/funder, who has granted bioRxiv a license to display the preprint in perpetuity. It is made available under a CC-BY-NC-ND 4.0 International license.

1 **Figure 1 | OpticSELINE design and fabrication**. **a**, Sketch of the OpticSELINE. The red box highlights
2 the connection area between the electrode and the flat cable terminated with an Omnetics connector
3 (not shown). The blue box highlights the active area where 2 flaps and 6 electrodes are visible.
4 Dimensions are in mm. **b**, Magnification of the active area after microfabrication. **c**, Enlarged view of
5 the flaps, electrodes, and alignment bars after three-dimensional shaping. **d**, Picture of one side of the
6 OpticSELINE. The electrode enlargement is used as a stopper to avoid excessive insertion of the array
7 within the nerve.
8
9 **Figure 2 | Electrochemical characterization**. **a**, Cyclic voltammetry performed on the electrodes
10 before (orange) and after (green) accelerated ageing. Representative example of 1 electrode with an
11 overlay of 10 repetitions. **b**, Quantification of the mean (± s.d.) charge storage capacity (n = 18). **c**,
12 Mean (± s.d.) magnitude (top) and phase (bottom) of the electrode impedances before (orange) and
13 after (green) accelerated ageing (n = 30). **d**, Quantification of the mean (± s.d.) impedance magnitude
14 at 1 kHz.
15
16 **Figure 3 | Mechanical characterization**. **a**,**b**, Scheme for the ex-vivo insertion (**a**) and extraction (**b**)
17 experiments in explanted optic nerves from New Zealand White rabbits. **c**, Forces during insertion in
18 the optic nerve. Several insertion trials (n = 10) are shown in grey while, in red, a selected example is
19 labelled with the different phases of insertion. Peak 1 is relative to the insertion of the loop and peak 2
20 is relative to the entry of the enlarged area. Mean (± s.d., n = 10) insertion forces are 32.5 ± 22.7 mN
21 (peak 1) and 223.4 ± 92.2 mN (peak 2). **d**, Forces during extraction from the optic nerve. Several
22 extraction trials (n = 10) are shown in grey while, in red, a selected example is labelled with the
23 different phases of extraction. Peaks (3 and 4) are relative to the extraction of the flaps and the flat
24 phase (5) is relative to the slippage of the loop through the nerve. Mean (± s.d., n = 10) extraction
25 forces are 101.2 ± 36.2 mN (peak 3) and 100.3 ± 38.5 mN (peak 4). **e**, The different phases of insertion
26 (1 and 2) are sketched. **f**, The different phases of extraction (3 to 5) are sketched.
27

bioRxiv preprint first posted online May. 7, 2018; doi: http://dx.doi.org/10.1101/311035. The copyright holder for this preprint (which was not peer-reviewed) is the author/funder, who has granted bioRxiv a license to display the preprint in perpetuity. It is made available under a CC-BY-NC-ND 4.0 International license.

1 **Figure 4 | Visually-evoked cortical potentials**. **a**, Recordings of VEPs have been performed with a
2 ECoG array covering the visual cortex and a flash stimulation (4 ms, white LED) in the ipsilateral
3 (black) or contralateral (red) eye. **b**, Example of traces (synchronous average of 10 responses) to a
4 flash illumination of 0.5 cd s m^{-2} at the ipsilateral (black) or contralateral (red) eye. The dashed lines
5 represent the occurrence of the flash. **c**, Example traces obtained from the average of the 32 recording
6 channels (showed in **b**) for both ipsi- (black) and contra- (red) lateral stimulation. P0, N1 and P1 peaks
7 are visible. The dashed lines represent the occurrence of the flash. **d**, Mean (± s.e.m.) of the P1 PAs
8 (left) and PLs (right) with respect to the flash luminance (N = 9). P1 PAs and PLs have been measured
9 in each rabbit from the average of the 32 recording channels.
10
11 **Figure 5 | Electrically-evoked cortical potentials**. **a**, EEPs have been evoked via the implanted
12 OpticSELINE with biphasic current pulses. **b**, Example of traces (synchronous average of 10 responses)
13 to a current pulse of 2 mA and 150 μs delivered from the electrode 6. The dashed lines represent the
14 occurrence of the current pulse. **c**, Example of traces (synchronous average of 10 responses) to
15 increasing current pulses of 150 μs from 1 recording electrode (red box in panel **b**). The appearance of
16 N1 and P1 peaks is visible. **d**, Mean (± s.e.m.) N1 activation thresholds in N = 1 rabbit depending on
17 pulse duration (circles, left y axis). The activation threshold is plotted also as charge delivered
18 (squares, right y axis). The dotted lines show the activation threshold for current pulses of 150 μs,
19 corresponding to 250 μA and 37.4 nC. **e**, Mean (± s.e.m.) amplitude of N1 (squares) and P1 (circles) for
20 current pulses of 150 μs with respect to the stimulation amplitude (N = 4). The insert shows a
21 magnification from 0 to 300 μA (x axis) and from 0 to 75 μV (y axis). **f**, Activation thresholds in N = 4
22 rabbits for current pulses of 150 μs (p = 0.86, Kruskal-Wallis). The dotted line represents the average
23 threshold (204.17 μA, N = 4). **g**, Mean (± s.e.m.) activation thresholds (N = 4; p = 0.25, one-way
24 ANOVA) depending on the electrode (from 1 to 6). In panels **d**, **e**, **f**, and **g**, the responses from the 32
25 recording electrodes have always been averaged. In panels **d**, **e**, and **f**, for each rabbit the
26 quantifications from each of the 6 electrodes (from 1 to 6) have been averaged.
27

bioRxiv preprint first posted online May. 7, 2018; doi: http://dx.doi.org/10.1101/311035. The copyright holder for this preprint (which was not peer-reviewed) is the author/funder, who has granted bioRxiv a license to display the preprint in perpetuity. It is made available under a CC-BY-NC-ND 4.0 International license.

1 **Figure 6 | Electrically-evoked cortical potentials with pulse trains**. **a**, EEPs have been evoked via
2 the implanted OpticSELINE with biphasic current pulses arranged in packages containing 1, 2, 3, or 4
3 pulses at 1 kHz of repetition rate. **b**, Normalized mean (± s.e.m.) of N1 activation threshold with stimuli
4 composed of 1 to 4 pulses (*N* = 4). The normalization has been performed with respect to the stimulus
5 with 1 pulse. **c**, Normalized means (± s.e.m.) of P1 PA (*N* = 4) for trains with 1, 2, 3, or 4 pulses (circles,
6 squares, triangles, and diamonds respectively). The normalization has been performed with respect to
7 the amplitude for 1 pulse at 1000 μA. In panels **b**, and **c**, the responses from the 32 recording
8 electrodes have always been averaged. Moreover, for each rabbit the quantifications from each of the 6
9 OpticSELINE electrodes (from 1 to 6) have been averaged.
10
11 **Figure 7 | Activation maps of the meaningful ICs**. **a**, Example of an activation map corresponding to
12 IC 1 projected in correspondence of the ECoG array. **b**, Example of the activation map, the PVAF, and
13 the time courses of a representative meaningful component (IC 1). A time course is shown for each
14 stimulating electrode of the OpticSELINE. **c**, The 26 meaningful ICs are present in distinct regions of
15 the visual cortex. Representative example from *N* = 1 rabbit with a current amplitude of 750 μA.
16
17 **Figure 8 | ICs distribution map at the level of the optic nerve**. **a,** Example of the distribution maps
18 of the first 4 meaningful ICs within the optic nerve. Enclosed in the red contour is the region of the
19 optic nerve which activation level is larger than 90% of the maximal activation. **b**, Overlay of the 90%
20 activation contours (red) of all the meaningful ICs. The dotted circle represents the optic nerve. The
21 sketch of the OpticSELINE is in black in both **a** and **b**. Representative example from *N* = 1 rabbit with a
22 current amplitude of 750 μA.

bioRxiv preprint first posted online May. 7, 2018; doi: http://dx.doi.org/10.1101/311035. The copyright holder for this preprint (which was not peer-reviewed) is the author/funder, who has granted bioRxiv a license to display the preprint in perpetuity. It is made available under a CC-BY-NC-ND 4.0 International license.

1 **Methods**

2 ***Electrode microfabrication***. The OpticSELINE was developed by using micro photolithography and
3 thin-film techniques. A silicon wafer was used as sacrificial layer. After the cleaning of silicon wafer
4 (10 min Acetone; DI rinse; 10 min Isopropanol), two layers of polyimide PI2610 (HD MicroSystems)
5 were spun on the substrate (2000 rpm for 30 s). Samples were hard baked in an oven with nitrogen
6 flux at 350 °C for 1 hr. LOL and S1813 (Microposit) were spin-coated on the wafer respectively at 1000
7 rpm for 20 s and 4500 rpm for 30 s. The substrate was exposed by using a glass photomask at a dose
8 of 180 mJ cm^{-2}. The sample was developed in MF319 for 30 s and rinsed in DI water. A layer of
9 titanium (20 nm) and gold (250 nm) were sputtered on the substrate and a lift-off technique was used
10 to release the pattern of traces, active sites and pads (overnight immersion in remover 1165). Two
11 layers of PI2610 were spun on the substrate (2000 rpm for 30 s) and hard baked in the oven with
12 nitrogen flux at 350 °C for 1 hr. An aluminum mask (200 nm) was deposited on the substrate by
13 thermal evaporation. S1813 was spun on the sample and exposed (glass photomask, 180 mJ cm^{-2}) and
14 the wafer was developed in MF319 for 30 s. S1813 was removed (2 min in remover 1165) and dry
15 etching was used to etch the excess of polyimide (40 sccm of O_2; 150 W, 1 hr). The aluminum mask
16 was etched away and electrodes were peeled off from the wafer. The three-dimensional geometry was
17 conferred to the OpticSELINE by securing the device on a stainless-steel mold. The mold has 4 holes in
18 correspondence of the 4 flaps; a needle was used to secure each flap inside the hole. Alignment holes
19 were included on the mold to ease the placement of the device. A thermal treatment (1 hr, 200 °C) was
20 used to memorize the curved shape of the flaps. The 3D devices were connected to the polyimide-
21 based extension cable: a silver conductive glue was used to connect the corresponding pads of the two
22 elements (Ablestik-Henkel; 1 hr at 130 °C). Then the flexible extension cable was connected to a
23 printed circuit board (PCB) by silver conductive glue. A surgical needle with a looped wire (Ethicon)
24 was inserted through the device. Flexible wires were soldered to the PCB and then a linear Omnetics
25 connector was attached. Two-component biocompatible silicone (Silbione-Bluestar Silicones) was
26 applied on all the soldering.

27 ***Electrochemical characterization***. Cyclic Voltammetry was performed using a three-electrode setup
28 immersed in phosphate-buffered saline (PBS) solution and applying a 10-cycle potential ramp at a

bioRxiv preprint first posted online May. 7, 2018; doi: http://dx.doi.org/10.1101/311035. The copyright holder for this preprint (which was not peer-reviewed) is the author/funder, who has granted bioRxiv a license to display the preprint in perpetuity. It is made available under a CC-BY-NC-ND 4.0 International license.

1 scan rate of 1.5 V s^{-1} between −0.5 V and 0.5 V. Impedance measurement was performed using a three-
2 electrode setup immersed in PBS solution and applying a sinusoid of 10 mV between 100 Hz and
3 100 kHz. Accelerated aging test was performed for 6 days at temperature of 87 °C with an
4 accelerating factor of 32. Different OpticSELINE arrays have been immersed in glass beakers filled
5 with PBS solution; the beakers were sealed and stored in oven.

6 ***Mechanical tests***. Both experiments were performed using the same setup composed of a press to
7 secure the nerve, a 10 N load cell, and an explanted rabbit optic nerve. During insertion experiments,
8 first the nerve was pierced by the needle, then the electrode was pulled at a constant speed of 15 mm
9 min^{-1} to insert the device inside the nerve. During extraction experiments, first the device was
10 implanted inside the nerve, then the electrode was pulled at a constant speed of 15 mm min^{-1} to
11 completely extract the device from the nerve. In both cases, insertion and extraction forces were
12 measured by a load cell.

13 ***Animal handling and surgery***. Animal experiments were performed under the animal authorization
14 GE1416. Female New Zealand White rabbits (> 16 weeks, > 2.5 kg) were sedated with an
15 intramuscular injection of xylazine (5 mg kg^{-1}). Anesthesia and Analgesia were provided with an
16 intramuscular injection of an anesthetic mix composed by: medetomidine (0.5 mg kg^{-1}), ketamine (25
17 mg kg^{-1}), and buprenorphine (0.03 mg kg^{-1}). If required, anesthesia was prolonged with a second
18 injection (half dose) of the anesthetic mix. Eye drops were placed on the eye to prevent eye drying.
19 The rabbit was placed on a heating pad at 35°C for the entire procedure. Oxygen was provided with a
20 mask to prevent hypoxia during the anesthesia. The head was shaved and cleaned with 70% ethanol
21 and betadine. The rabbit's head was then secured gently within a stereotactic frame (David Kopf
22 Instruments). Prior to cortical skin incision, a mix of lidocaine (6 mg kg^{-1}), bupivacaine (2.5 mg kg^{-1}),
23 and epinephrine (0.1 mg kg^{-1}) was injected subcutaneously on the surgical sites. After 5 minutes, the
24 skin was opened and pulled aside to expose the skull; finally, the skull was cleaned with cotton swabs.
25 First a temporal craniotomy was made to access the left optic nerve. The OpticSELINE was inserted in
26 the left optic nerve from lateral to medial in the pre-chiasmatic area. Then a second craniotomy was
27 made to expose the right visual cortex. A32-channel epi-dural ECoG array (E32-1000-30-200;
28 NeuroNexus) was placed on the visual cortex. All rabbits were euthanized at the end of the acute

bioRxiv preprint first posted online May. 7, 2018; doi: http://dx.doi.org/10.1101/311035. The copyright holder for this preprint (which was not peer-reviewed) is the author/funder, who has granted bioRxiv a license to display the preprint in perpetuity. It is made available under a CC-BY-NC-ND 4.0 International license.

1 recording procedures, while still under anesthesia, with an intravenous injection of pentobarbital (120
2 mg kg^{-1}).
3 ***Optic nerve anatomy***. To determine the average nerve diameter, optic nerves (*n* = 10) were explanted
4 from 5 female New Zealand white rabbits (> 16 weeks, > 2.5 kg), immediately embedded in the
5 optimum cutting temperature compound (O.C.T. Tissue-Tek, Qiagen), and frozen at -20 °C. 10-μm
6 sections were obtained with a cryostat (Leica Microsystems) and mounted on glass slides. Images
7 were taken with a slide scanner (VS120-L100, Olympus).
8 For the myelin staining, the optic nerve was extracted after surgery and fixed overnight in PFA 4%.
9 The tissue was then dehydrated with increasing concentrations of ethanol and embedded in paraffin.
10 5-μm thick sections were cut using a microtome (Leica Microsystems) in the portion close to the optic
11 chiasma. The Woelcke staining for myelin was performed on the sections after dewaxing by
12 specialized technicians and the images acquired in transmitted light at 40X magnification and
13 analyzed using ImageJ.
14 For the myelin basic protein staining, antigen retrieval in citrate buffer (pH 6) was performed on
15 dewaxed sections. The samples were then blocked for one hour in PBS-Triton 0.1 % + NGS 5 %
16 (Jackson Immuno Research) and incubated at 4 °C overnight with the primary antibody (rabbit anti-
17 MBP 1:200, ab40390, Abcam). The following day, the sections were washed in PBS and incubated 1
18 hour at room temperature with the secondary antibody (goat anti rabbit Alexa-488). The samples
19 were mounted for imaging using Fluoromount (Sigma-Aldrich) solution. The images were acquired
20 with a confocal microscope (LSM-880, Carl Zeiss) at 63 X magnification and analyzed using ImageJ.
21 ***Electrophysiology***. For optic nerve stimulation the OpticSELINE was attached to a current stimulator
22 (IZ2MH; Tucker-Davis Technologies), while for cortical recordings the ECoG array (E32-1000-30-200;
23 NeuroNexus) was connected to an amplifier (PZ5; Tucker-Davis Technologies) via a 32-channels
24 analog headstage (ZIF-Clip® Analog Headstage; Tucker-Davis Technologies). Optic nerve stimulation
25 was performed with 13 pulse amplitudes (10, 25, 50, 75, 100, 150, 200, 250, 500, 750, 1000, 1500, and
26 200 μA) and 5 pulse durations (50, 100, 150, 200, and 400 ms) delivered in a scrambled manner. Data
27 were filtered between 0.5 Hz and 2 kHz and digitalized at 12 kHz. Epochs (from –100 to 750 ms)

bioRxiv preprint first posted online May. 7, 2018; doi: http://dx.doi.org/10.1101/311035. The copyright holder for this preprint (which was not peer-reviewed) is the author/funder, who has granted bioRxiv a license to display the preprint in perpetuity. It is made available under a CC-BY-NC-ND 4.0 International license.

1 synchronous to the onset of the stimulation were then extracted from the data stream and data
2 analysis was performed with Matlab (Mathworks).
3 ***Blind source separation***. For each recording electrode and each stimulation intensity, epochs were
4 concatenated and processed with an AMICA [48] core and GPU-processed infomax reliable ICA (RELICA)
5 algorithm [49] . Dimensionality reduction on the data as a preprocessing step to ICA was not performed [50]
6 . RELICA allowed to test the repeatability of ICs appearing in decompositions of bootstrapped versions
7 of the input data and to retain only stable ICs for further analysis. Given the multivariate dataset from
8 the 32 recording electrodes X(electrode, time), ICA extracts an unmixing matrix W (32 x 32) such that
9 the IC time courses S=WX are maximally independent. Rows of W represent the weights applied to
10 each electrode to obtain the corresponding ICs *S*. The column i^{th} of the mixing matrix A (pseudoinverse
11 of W) represents the weight of the ith IC on each recording electrode and can be represented as an
12 activation map. Each activation map was obtained by projecting the weights of the unmixing matrix A
13 onto the layout of the ECoG array, then by spatially interpolating them with a spline-function, and
14 finally by normalizing the maps to the maximal absolute value present in the interpolated map. IC
15 grand average time courses, obtained by performing the average over trials for each stimulation
16 intensity, formed the IC-EEPs. The percent of variance accounted for (PVAF) by each IC on each
17 electrode was computed and represented as a PVAF activation map. ICs were categorized into several
18 classes, namely: flat, common, artifact, noise, and meaningful (**Supplementary Fig. 4a**). First, low
19 frequency components of the signal were removed using a zero-phase high-pass filter with a 5 Hz cut-
20 off frequency. Then artifact ICs, exhibiting a large activation within the first 5 ms from the stimulus
21 onset, were identified by visual inspection and removed. To verify that the artifact ICs were correctly
22 identified, all the other ICs were back-projected. The initial portion of the back-projected signal (0 to 5
23 ms) was indeed exclusively affected by the manual removal of the artifact ICs when compared to the
24 original signal (**Supplementary Fig. 9**). Following the identification of the artifact, the noise ICs were
25 identified by computing the frequency plot of the signal; the ICs exhibiting unusual peaks in the 250 to
26 500 Hz frequency range were labeled as noise (**Supplementary Fig. 4b**). Amongst the remaining ICs
27 (**Supplementary Fig. 4c**), the ones with a peak-to-peak variation (Δ) in the time course (time frame
28 from 5 to 25 ms after the stimulus) smaller than 3 times the standard deviation of the time course (σ)

bioRxiv preprint first posted online May. 7, 2018; doi: http://dx.doi.org/10.1101/311035. The copyright holder for this preprint (which was not peer-reviewed) is the author/funder, who has granted bioRxiv a license to display the preprint in perpetuity. It is made available under a CC-BY-NC-ND 4.0 International license.

1 were labelled as flat ($\Delta/\sigma < 3$). To separate meaningful ICs from common ICs, a similarity index was
2 used; that is the correlation between the time courses of the different stimulating electrodes. ICs were
3 classified as common (i.e. with visible meaningful activation but with similar time courses for all the
4 stimulating electrodes) for a mean similarity index larger than 0.4. Distribution maps in the optic
5 nerve were obtained by interpolating with a spline function the contribution of every stimulating
6 electrodes to each IC. The contour of the optic nerve was set to zero.
7 ***Statistical analysis and graphical representation***. Statistical analysis and graphical representation
8 were performed with Prism (GraphPad Software Inc.). The normality test (D'Agostino & Pearson
9 omnibus normality test) was performed in each dataset to justify the use of a parametric or non-
10 parametric test. In each figure p-values were represented as: * $p < 0.05$, ** $p < 0.01$, *** $p < 0.001$, and
11 **** $p < 0.0001$. Data are reported as mean ± s.e.m. or mean ± s.d., *n* is used to identify the number of
12 electrodes used; *N* is used to identify the number of animals.
13 ***Data availability.*** The authors declare that all other relevant data supporting the findings of the study
14 are available in this article and in its Supplementary Information file. Access to our raw data can be
15 obtained from the corresponding authors upon reasonable request.

a

33

3

Reference

Ground

Extension flat cable

3

35

Active area

0.48

0.43

0.1

0.15

0.43

0.22 0.22 0.18

1.25

b

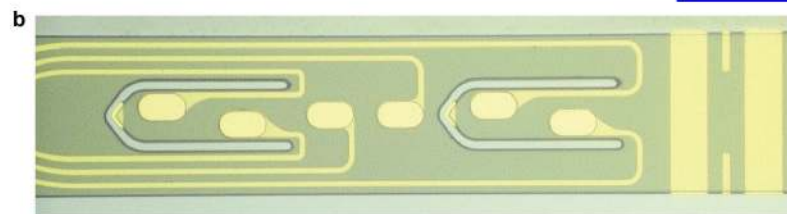

c

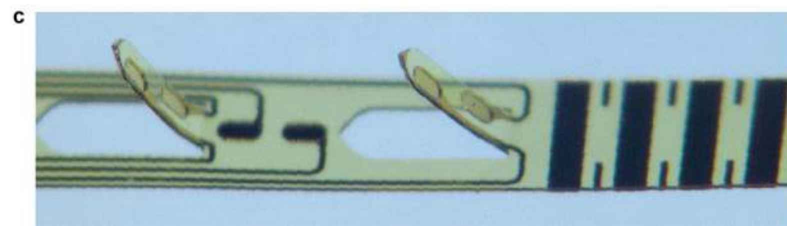

d

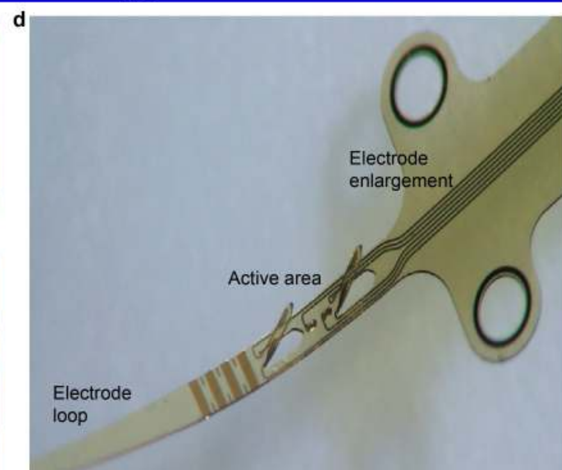

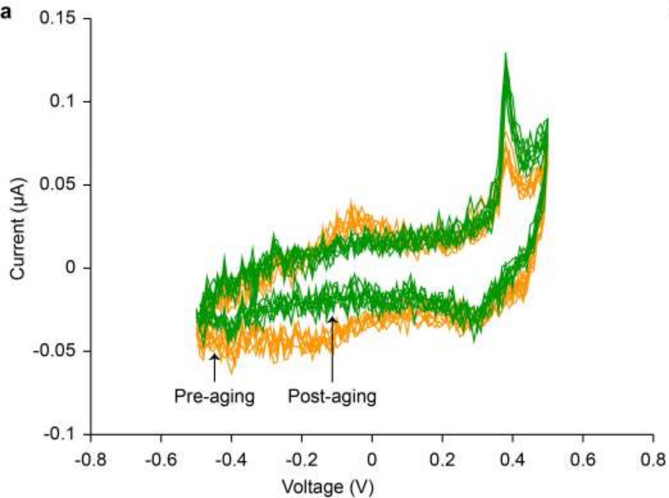
a
Current (μA)
Voltage (V)
Pre-aging
Post-aging
0.15
0.1
0.05
0
-0.05
-0.1
-0.8
-0.6
-0.4
-0.2
0
0.2
0.4
0.6
0.8

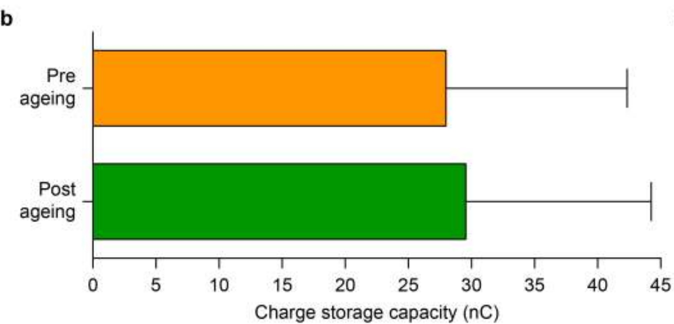
b
Pre
ageing
Post
ageing
Charge storage capacity (nC)
0
5
10
15
20
25
30
35
40
45

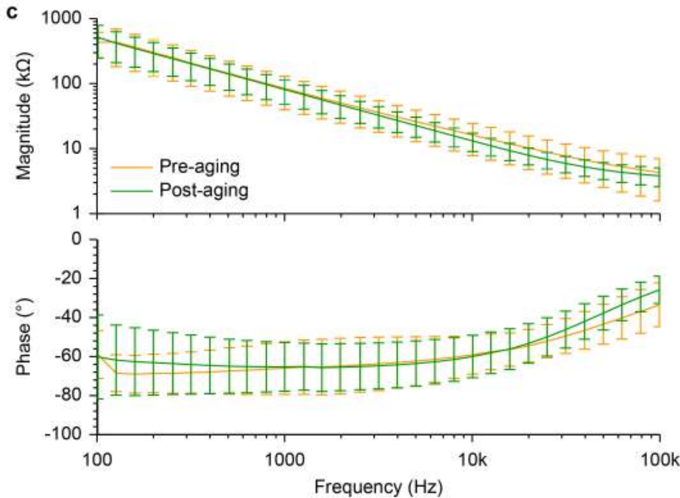
c
Magnitude (kΩ)
Pre-aging
Post-aging
1000
100
10
1
Phase (°)
0
-20
-40
-60
-80
-100
Frequency (Hz)
100
1000
10k
100k

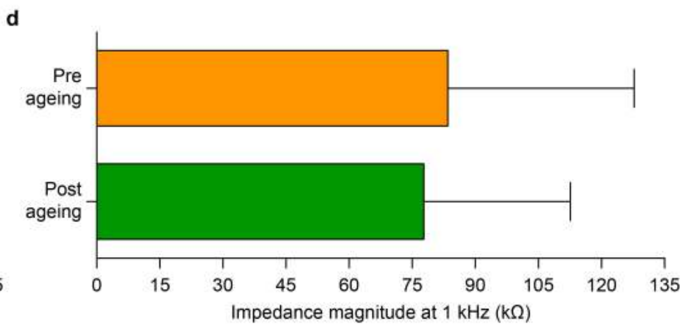
d
Pre
ageing
Post
ageing
Impedance magnitude at 1 kHz (kΩ)
0
15
30
45
60
75
90
105
120
135

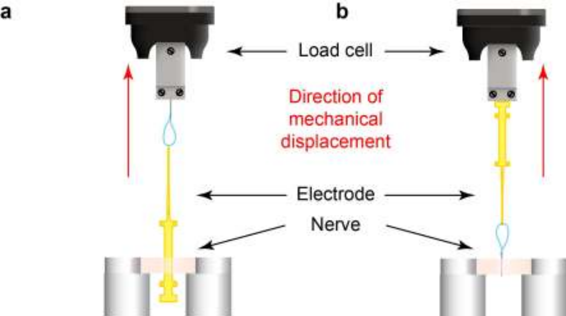
a
b
Load cell
Direction of mechanical displacement
Electrode
Nerve

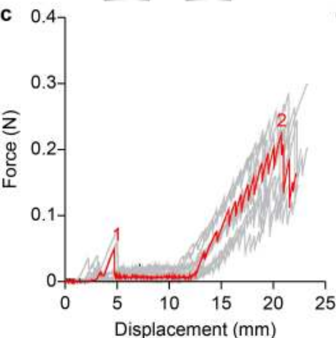
c
Force (N)
Displacement (mm)
1
2

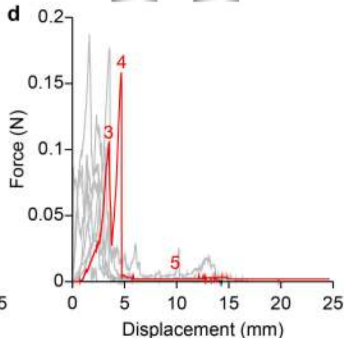
d
Force (N)
Displacement (mm)
3
4
5

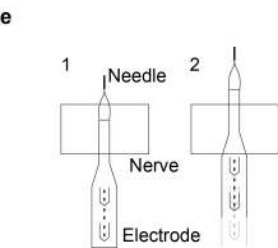
e
1
2
Needle
Nerve
Electrode

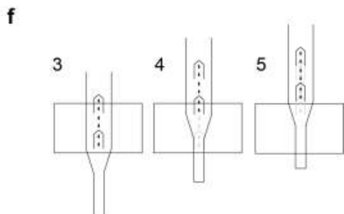
f
3
4
5

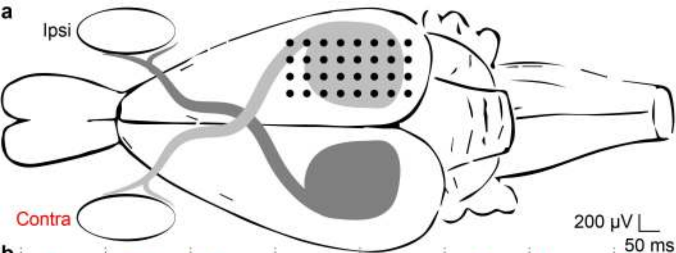
a
Ipsi
Contra
200 μV
50 ms
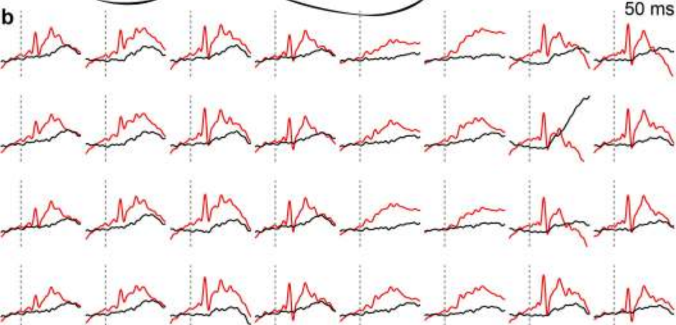
b
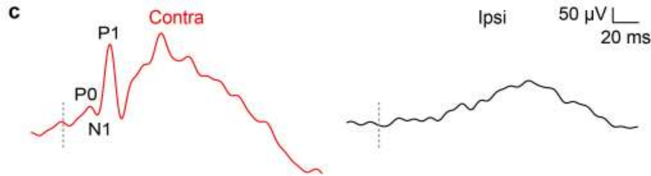
c
Contra
P1
P0
N1
Ipsi
50 μV
20 ms
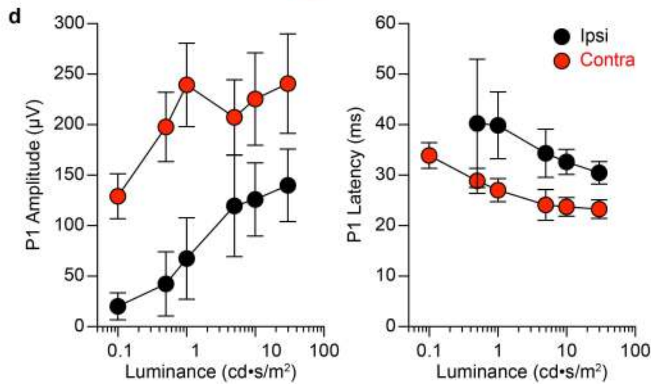
d
P1 Amplitude (μV)
Luminance (cd•s/m²)
P1 Latency (ms)
Luminance (cd•s/m²)
Ipsi
Contra

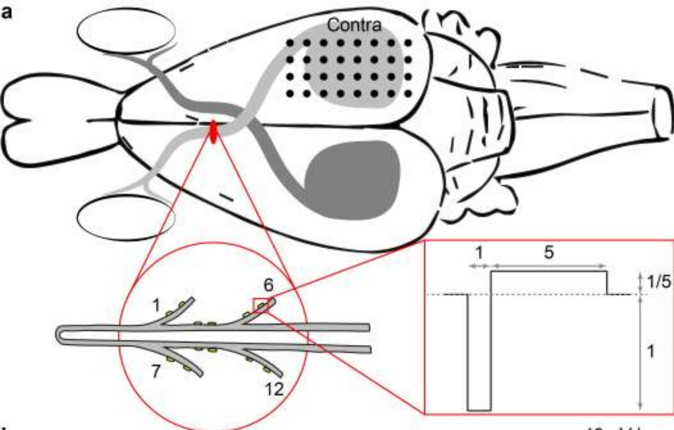
a
Contra
1
5
1/5
1
6
1
7
12

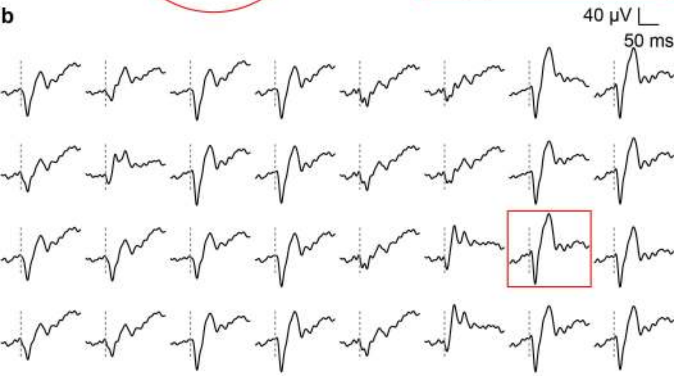
b
40 µV
50 ms

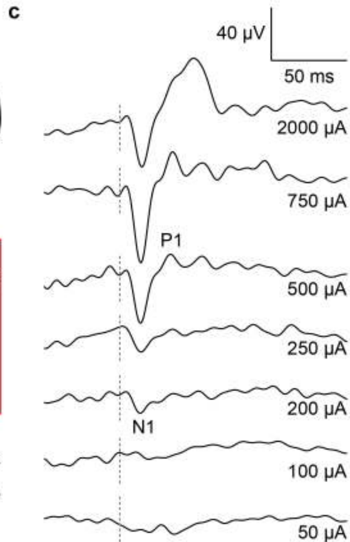
c
40 µV
50 ms
2000 µA
750 µA
P1
500 µA
250 µA
200 µA
N1
100 µA
50 µA

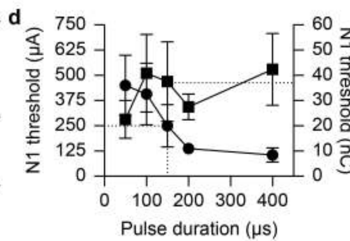
d
N1 threshold (µA)
N1 threshold (nC)
Pulse duration (µs)

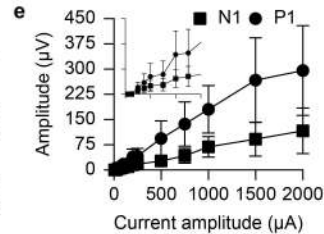
e
N1
P1
Amplitude (µV)
Current amplitude (µA)

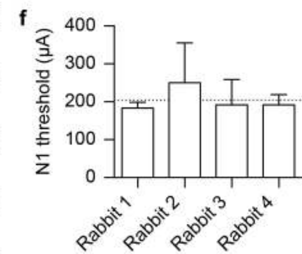
f
N1 threshold (µA)
Rabbit 1
Rabbit 2
Rabbit 3
Rabbit 4

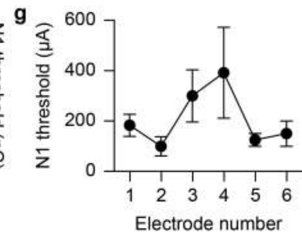
g
N1 threshold (µA)
Electrode number

a

Contra

1

6

7

12

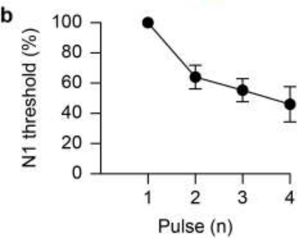

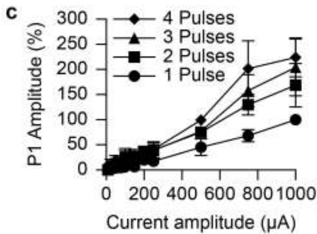

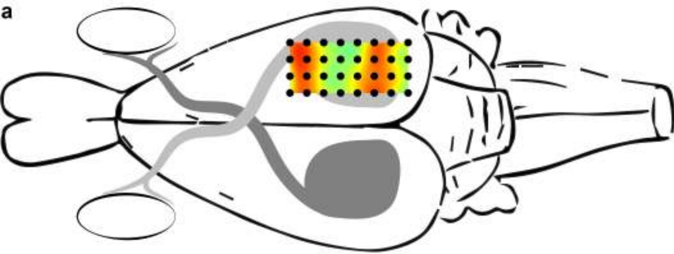
a

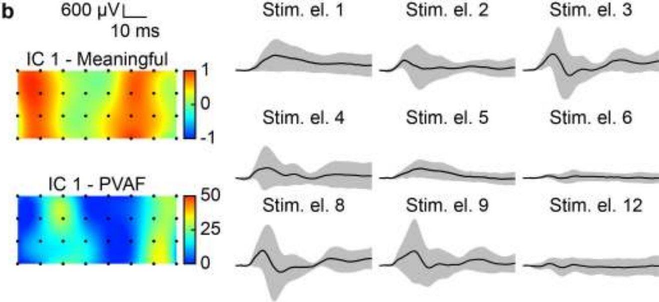
b
600 µV
10 ms
IC 1 - Meaningful
1
0
-1
IC 1 - PVAF
50
25
0
Stim. el. 1
Stim. el. 2
Stim. el. 3
Stim. el. 4
Stim. el. 5
Stim. el. 6
Stim. el. 8
Stim. el. 9
Stim. el. 12
c
1
2
3
6
7
8
9
10
11
12
13
16
17
18
19
20
21
22
23
24
26
27
28
30
31
32
-1
-0.8
-0.6
-0.4
-0.2
0
0.2
0.4
0.6
0.8
1

a

Meaningful IC1

Meaningful IC2

Meaningful IC3

Meaningful IC6

1 0.9 0.8 0.7 0.6 0.5 0.4 0.3 0.2 0.1 0

b